SafeLand

Living with landslide risk in Europe: Assessment,
effects of global change, and risk management strategies

7th Framework Programme
Cooperation Theme 6 Environment (including climate change)
Sub-Activity 6.1.3 Natural Hazards

Deliverable 3.3

Analysis of selected extreme precipitation events with the COSMO-CLM model on a spatial scale of 2.8 km

Work Package 3.1 – Climate change scenarios for selected regions in Europe

Author: Edoardo Bucchignani - CMCC

March 2012

Rev.	Deliverable Responsible	Controlled by	Date
0	CMCC		September 2011
1	CMCC	MPI-M	November 2011
2	CMCC	MPI-M	March 2012

INDEX

Introduction

The main aims of the WP 3.1 of the SAFELAND project are the following:

- to provide basic information about the expected climate changes in Europe, with special focus on heavy precipitation events, at a spatial resolution of about 25 *km*, based on a multi-model ensemble;
- to provide high-resolution climate change projections on a spatial scale of 10 *km* for four selected regions in Europe and investigate meteorological extreme events;
- to provide climate projections at a very high spatial resolution (about 2.8 *km*) and investigate changes in meteorological extreme events.

The high attention of the scientific and social community for these applications is due to the expected increase of natural hazards as a consequence of climate change; for example, an expected increase of the temperatures, accompanied by a reduction of precipitation, could produce a decrease of the net infiltration that strongly influences the soil stability. One of the conclusions of the IPCC Fourth Assessment Report (AR4, Solomon 2007 [6]) is that there are evidences that climate change affects the frequency, intensity, and length of many extreme events, such as floods, droughts, storms and extreme temperatures. At the same time, changes in ecosystems and natural resources further enhance the consequences of extreme weather events.
Extreme weather events are, by definition, rare events and obey different statistical laws than averages (Naveau et al., 2005 [4]). Extreme value theory tackles the problem to estimate the probability distributions of rare events. Depending on the data basis and the purpose of the analysis, different statistical methods are appropriate. When data values are available at a daily basis over a certain time period, as in this study, it is of large interest, to keep as much information as possible about the extreme daily events. An adequate method is therefore the "Peaks-over-threshold" approach in which extreme events are considered as exceedances over a high threshold. A statistical model, the Generalized Pareto Distribution, is fitted to the exceedances over the threshold, which in this study is the empiric value of the 95^{th} percentile. The distribution is formed by two parameters, one describing its shape and one describing its scale. Instead of looking at the parameter values themselves, return levels are calculated, which are more convenient to interpret. In this study the return levels of daily precipitation totals with a 10-year return period are determined for the time periods 1971-2000, regarded as representative for the present climate and 2021-2050, regarded as representative for the future climate. A more detailed description of the Peaks-over-threshold approach and the Generalized Pareto Distribution can be found e.g. in Coles, 2001 [1].
The activities related to the first two goals of this WP have been carried out at the Max Planck Institute for Meteorology (MPI-M), Germany: a statistical analysis of an ensemble of regional climate change simulations has been executed, with the aim of evaluating an estimation of intensity and frequency variation of future extreme events. The regional climate model simulations with a spatial resolution of 25 *km* and employing the SRES A1B emission scenario were carried out by several European research centres in the framework of the EU FP6 project ENSEMBLES. This scenario describes a future world with rapid economic growth and population increase until 2050. Furthermore, new and more efficient technologies are assumed to be developed. In the A1B scenario, the energy supply is balanced across non-fossil and fossil sources. From the same project, the simulations of the regional climate model REMO have been used by MPI-M to produce the

boundary and initial conditions for other simulations (always with REMO) at 10 *km* resolutions on three European regions, namely “Italy and Alps”, “Northern Europe“ and “Eastern Europe”.
Finally, for specific applications on particular kinds of landslides, the 10 *km* resolution is not yet sufficient: for this reason, a double nesting procedure has been performed: the results obtained with REMO at 10 *km* resolutions have been provided to CMCC and used to generate the boundary and initial conditions to perform simulations at very high resolution using the regional climate model COSMO-CLM: in this way, a physically consistent simulation of small scale climatic features, e.g., local precipitation extremes and other landslide triggering events, is possible and can be linked to geo-mechanical models used for high resolution case studies in other work packages.
The CMCC is in charge of the last goal of this WP: the mentioned high resolution simulations have been performed on four areas selected inside the three European regions mentioned above. Unfortunately, it was not possible to perform the simulations with a spatial resolution of 2.8 *km*, because the values of external parameters needed by the model were not available at this resolution: so a value of 3.8 *km* was adopted. The output of the simulations has been provided to some partners of the project SAFELAND.
This document is organized as follows: Chapter 1 contains a description of the numerical model COSMO-CLM and of the procedure used to perform the dynamical downscaling from the REMO output. Chapter 2 contains a description of the method and the performed test cases. Chapter 3 contains the analysis of the results for the four test cases. The main conclusions follow at the end of the document.

1 The COSMO-CLM model

1.1 General description

COSMO-CLM [5] is a non-hydrostatic limited area atmospheric prediction model for climatological applications. It can be used for simulations on time range up to a century, with a spatial resolution between 1 and 50 *km*; at such resolutions, orography is better described with respect to the global models, where there is an over/underestimation of valley/mountain heights resulting in errors for orographic precipitation estimation, which is closely related to terrain height.

COSMO-CLM has been developed by the DWD–Germany and by the COSMO consortium for weather forecast services. The model has been successively updated by the CLM-Community, for the application to climate simulations.

Convection can redistribute significant amounts of moisture, heat and mass on small temporal and spatial scales. Furthermore convection can cause severe precipitation events (as thunderstorms or cluster of thunderstorms). Being a subgrid scale phenomenon, the convection usually has to be parameterized. In the CLM code, different convection schemes, such as the Tiedtke scheme [7], and the Kain-Fritsch scheme [3], are implemented. The choice of this parameterization is essential in order to simulate the convective phenomena as the strong convective summer precipitation; these last ones, in fact, may cause flash floods because the heavy rain falling on bare soil and rocks runs off much faster than in winter, when vegetation is present. The mathematical formulation of COSMO-CLM is made up of the Navier-Stokes equations for a compressible flow. The atmosphere is treated as a multicomponent fluid (made up of dry air, water vapour, liquid and solid water) for which the perfect gas equation holds, and subject to gravity and to the Coriolis forces. The model includes several other “parameterizations”, in order to keep into account, at least in a statistical

manner, several phenomena that take place on unresolved scales, but that have significant effects on the meteorological scales of interest (for example, interaction with the orography). Further parameterizations are available in order to describe some important physical phenomena for the atmospheric evolution, for example solar radiation, precipitation, soil behaviour and microphysics.

The governing equations can be written as follows [2]:

$$\rho \frac{d\vec{v}}{dt} = -\nabla p + \rho g - 2\Omega \times (\rho \vec{v}) - \nabla \cdot \bar{t}$$

$$\frac{dp}{dt} = -(c_p / c_v)\, p \nabla \cdot v + (c_p / c_v - 1) Q_h + (c_p / c_v) Q_m$$

$$\rho c_p \frac{dT}{dt} = \frac{dp}{dt} + Q_h$$

$$\rho \frac{dq^x}{dt} = -\nabla \cdot J^x + I^x$$

$$p = \rho R_d (1 + \alpha) T$$

in which $\vec{v}$ is the velocity vector, ρ is the density, p is the pressure, g is the gravity acceleration, Ω is the constant angular velocity of earth rotation, $\vec{t}$ is the stress tensor due to viscosity, c_v and c_p are the specific heat of moist air, respectively at constant volume and constant pressure. Q_h and Q_m are respectively the heat production per unit volume of air and the impact of changes in the concentrations of the humidity constituents on the pressure tendency. Moreover, T is the temperature, q^x are the mass fractions of the constituents of the mixture (i.e. $x = d, v, l, f$ respectively for dry air, water vapour, liquid water and frozen water), J_x and I_x are, respectively, the source/sink and the diffusion flux of the constituent x and R_d is the gas constant for dry air. The moisture term α is defined as $\alpha = (R_v / R_d - 1) q^v - q^l - q^f$, where R_v is the gas constant for water vapour.

The discretization of the fluid dynamics equations is performed by using finite difference approximation, on a computational grid defined in a rotated spherical coordinate system. The pole is tilted and can be positioned such that the equator runs through the centre of the model domain. Problems resulting from the convergence of the meridians can be minimized for any limited area model domain on the globe. Especially, for a very small domain with negligible impact of the curvature of the earth's surface, the equations become identical to those for a tangential Cartesian coordinate system. Three time integration algorithms are available: the first one is based on a second order accurate Runge-Kutta method on two time levels; the second is based on the "horizontal explicit - vertical implicit" variant of Leapfrog scheme, the third based on a semi-implicit Leapfrog scheme on three time levels. The parallelization is done by horizontal and vertical domain decomposition: the Interface software MPI is used as Message Passing.

COSMO-CLM considers limited domains, so it is not possible to impose physical boundary conditions: they are therefore obtained from another climate model (global or regional) in a numerical manner by means of a dynamical *downscaling* technique. In this work, as already explained, boundary conditions have been obtained from the results of the REMO model.

1.2 Dynamic downscaling from REMO simulation

The solutions of the regional climate model REMO are saved in IEG format files and are used to generate the boundary and initial conditions to perform simulations at very high resolution (3.8 *km*) with the regional climate model COSMO-CLM. The latter uses the software INT2LM that reads the output files of a lower resolution model (global or regional) and calculates the boundary conditions for the domain under study at the desired resolution.. INT2LM is able to manage GRIB or NETCDF files. For this reason, it is necessary to use a suitable procedure, named IEG2NC, that converts the IEG files into the NETCDF format. The data flow chart is shown in Figure 1.2.1.

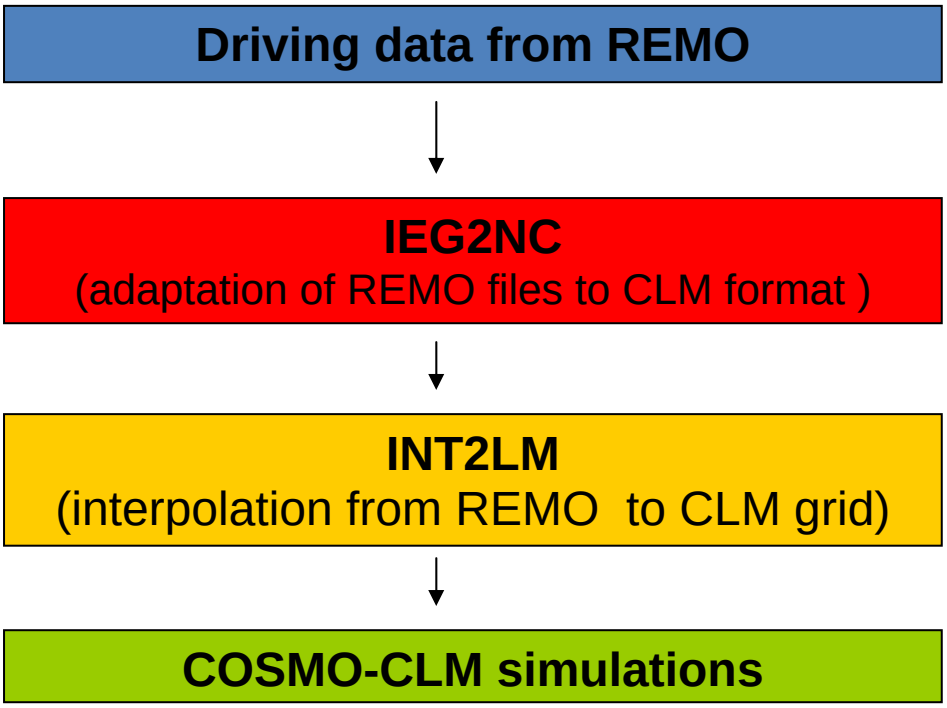

Figure 1.2.1: The data flow chart from REMO to COSMO-CLM

2. Description of the simulations performed

The COSMO-CLM simulations have been performed on four domains, listed in the following table.

Test Nr.	Country	Location	Reference geographical coordinates
1	Norway	Nedre Romerike	NW corner: E 10.73° N 60.36° SE corner: E 11.47° N 59.76°
2	Italy	Pizzo d'Alvano, Campania	Central point E 14.634° N 40.834°
3	France	Barcellonette Department of Alpes-de-Hautes-Provence,	NW corner: E 6°30.00 N 44°26.50 SE corner: E 6°52.35 N 44°19.30
4	Romania	Telega	Central point E 25.783° N 45.133°

On each of these domains, a computational grid with *80 x 80* nodes has been defined (resolution *3.8 km*), in order to cover an area of about 300 *km* x 300 *km*, centred on the points of interest listed in the previous table.
The time step has been set equal to 40 *sec*, employing a Runge-Kutta 2-time level HE-VI integration as numerical scheme. The observed period is 1951-2050, employing the SRES-A1B scenario.

The following parameterization schemes have been adopted:

- Radiation: the interaction of solar and thermal radiation with optically active constituents of the atmosphere. Computes heating rates in the atmosphere and energy balance at the ground (scheme of Ritter and Geleyn, 1992)
- Grid scale precipitation (cloud microphysics): computes the effects of precipitation formation on temperature and moisture variables in the atmosphere (scheme developed at DWD)
- Moist convection: includes subgrid scale convection and its effects on temperature, water vapor and wind (scheme of Tiedtke, 1989)
- Vertical turbulent diffusion: 1-D Prognostic TKE-based scheme
- Surface fluxes: these fluxes provide a coupling between the atmospheric part of the model and the soil model (TKE-based surface transfer scheme)
- Soil processes: multilayer deep soil scheme, including melting processes within the soil. Computes the temperature and specific humidity at the ground.

3. Analysis of the results

For the four selected locations, the daily values of the two-metre temperature (^oC) and of the total precipitation (*mm/month*) have been evaluated and averaged over the period 1971-2000 (baseline reference period), subdivided by seasons (winter DJF and summer JJA). The same distributions have been analyzed over the future period 2021-2050 and compared with the ones related to the past, in order to highlight changes of these climatic variables.
An analysis of extreme precipitation events has also been performed. Source of precipitation are mainly large synoptic systems but, especially during summer, strong convective storms might play a fundamental role. In order to characterize the extreme events of precipitation and their changes, the histogram in selected points of the domains has been evaluated (for the past and for the future period). Moreover, in order to better quantify the variation of extreme precipitation, the 10-year return levels (*mm/day*) related to the past period 1971-2000 and to the future period 2021-2050 have been evaluated.

3.1 Test case 1: Nedre Romerike (Norway)

This paragraph contains a description of the results related to the test case 1 (Nedre Romerike, Norway). The location is shown in Fig. 3.1.1 (taken from Google Earth).

Climate of the period 1971-2000 and climate projections over 2021-2050

Fig. 3.1.2 shows the climatology of two-metre temperature over the period 1971-2000 for winter (left) and summer (right). Similarly, Fig. 3.1.3 shows the distribution of total precipitation for winter (left) and summer (right). Fig. 3.1.4 shows the variation of two-metre temperature obtained by subtracting the average values on the period 2021-2050 from the average values on the period 1971-2000 for winter (left) and summer (right). Strong increases (up to 3.2^o C) are expected in winter, and between *1* and 2^o C in summer, over the whole area.
Fig. 3.1.5 shows the variation of total precipitation (future vs. past) for winter (left) and summer (right). A general increase of precipitation is projected in winter; in summer the western part of the domain shows a reduction, while the eastern part shows a slight increase of precipitation.
Figure 3.1.6 shows the histogram of precipitation (past and future period) in the central part of the domain, for winter (left) and summer (right). It is evident that the number of precipitation events above 50 mm is larger in summer but is projected to slightly increase in both the seasons, especially in winter.

Analysis of extreme events

Figure 3.1.7 shows the spatial pattern of the 10-year return levels for the period 1971-2000 for winter (left) and summer (right). The analysis of these pictures shows that strongest precipitation events occur in the north-west part of the domain, without significant differences between the two seasons. Similarly, Figure 3.1.8 shows the changes of the 10-year return levels for the period 2021-2050 with respect to 1971-2000, for winter (left) and summer (right): similar patterns are obtained

for both the seasons, with a general increase of extreme events, which is strongest in the western part of the domain, where the strongest precipitation events are simulated.

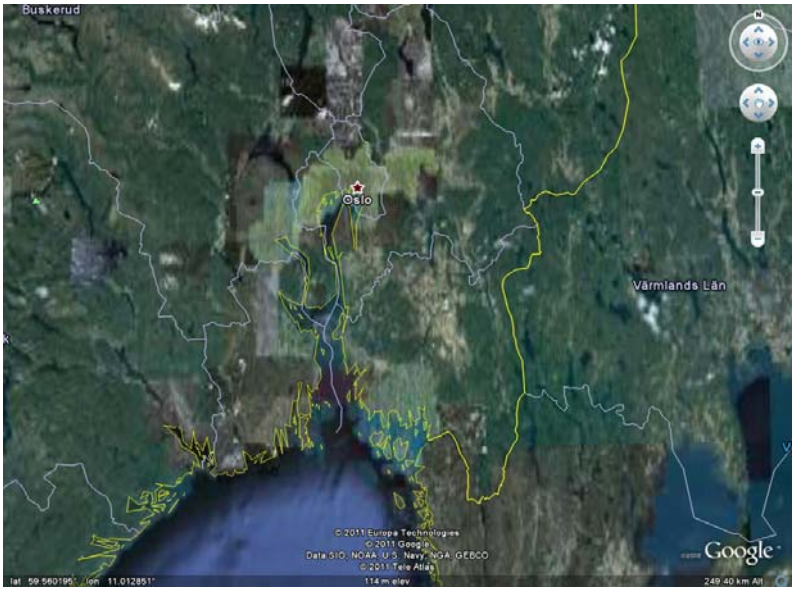

Figure 3.1.1: Location of the site related to test case 1.

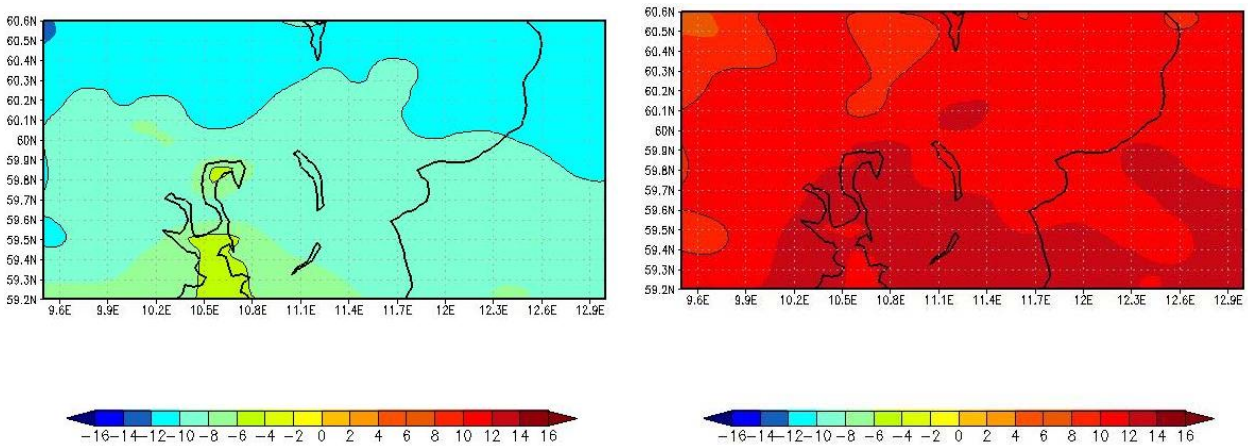

Figure 3.1.2: Two-metre temperature (^oC), averaged on the time period 1971-2000, for winter (left) and summer (right).

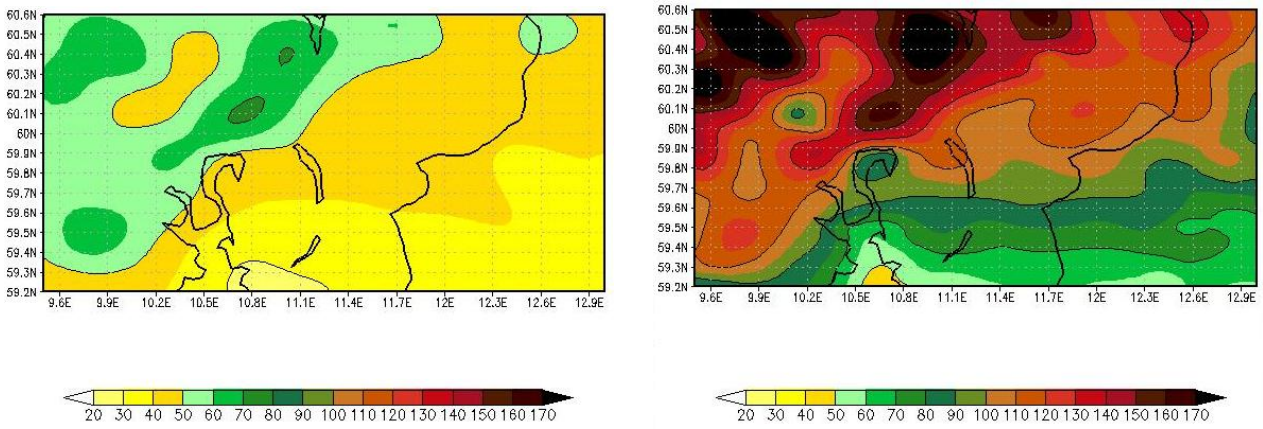

Figure 3.1.3: Total precipitation (*mm/month*), averaged on the time period 1971-2000, for winter (left) and summer (right).

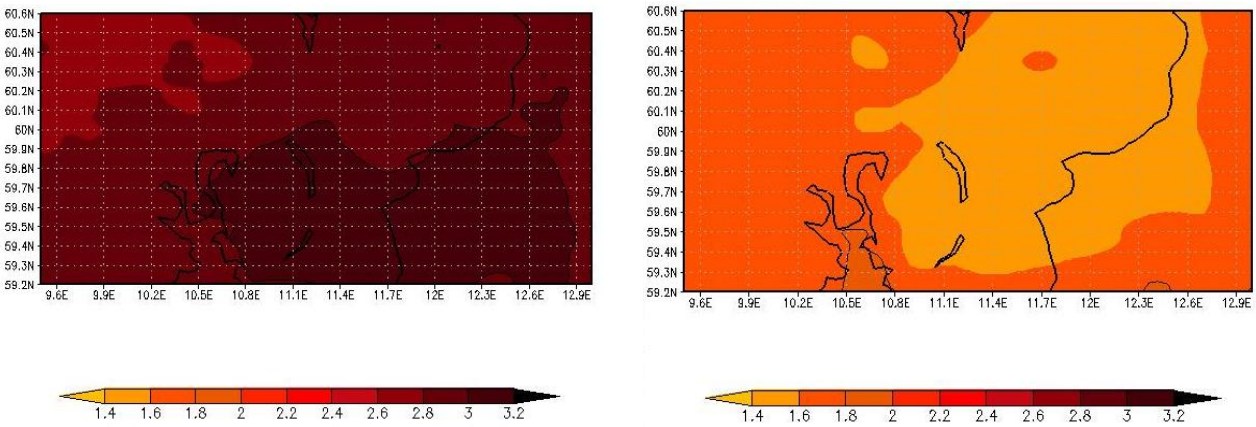

Figure 3.1.4: Change of two-metre temperature (^oC): average values on the period 2021-2050 minus average values on period 1971-2000, for winter (left) and summer (right).

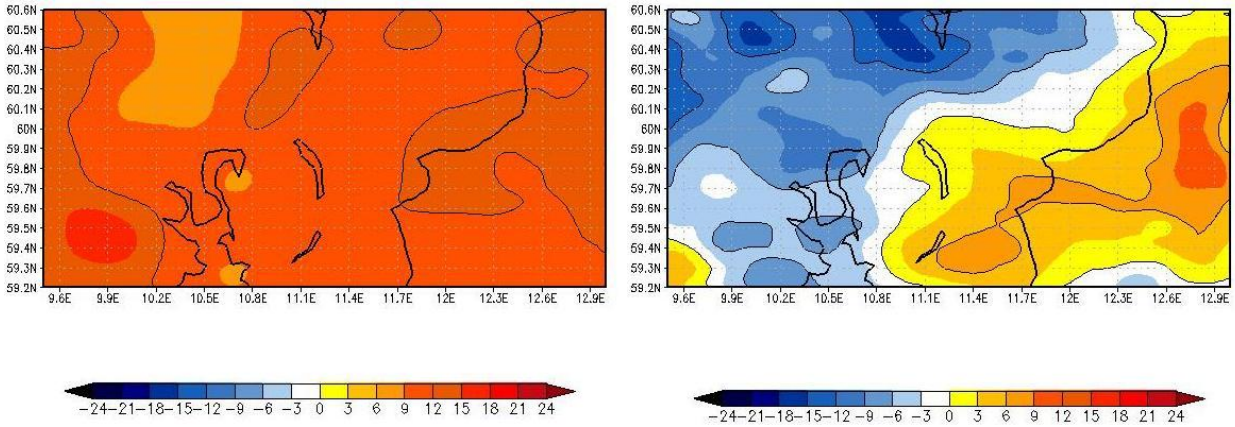

Figure 3.1.5: Change of total precipitation (*mm/month*): average values on the period 2021-2050 minus average values on period 1971-2000, for winter (left) and summer (right).

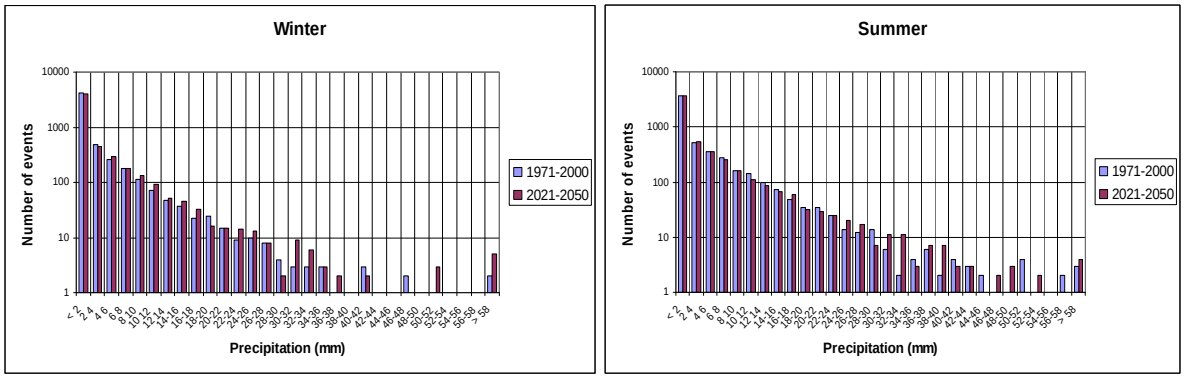

Figure 3.1.6: Histogram of daily total precipitation related to the central part of the domain for winter (*left*), summer (*right*), periods 1971-2000 and 2021-2050.

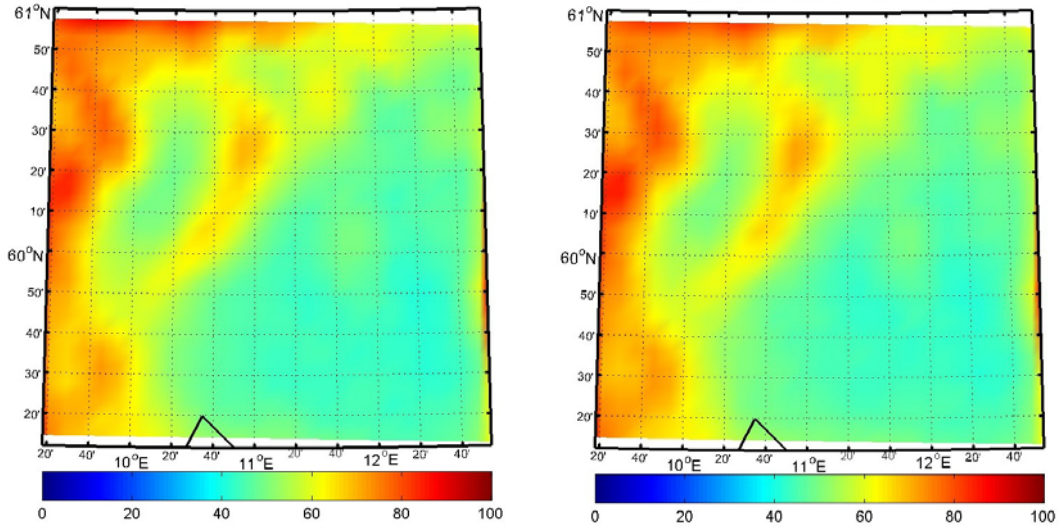

Figure 3.1.7: 10-year return levels (*mm/day*) related to the period 1971-2000, for winter (left) and summer (right).

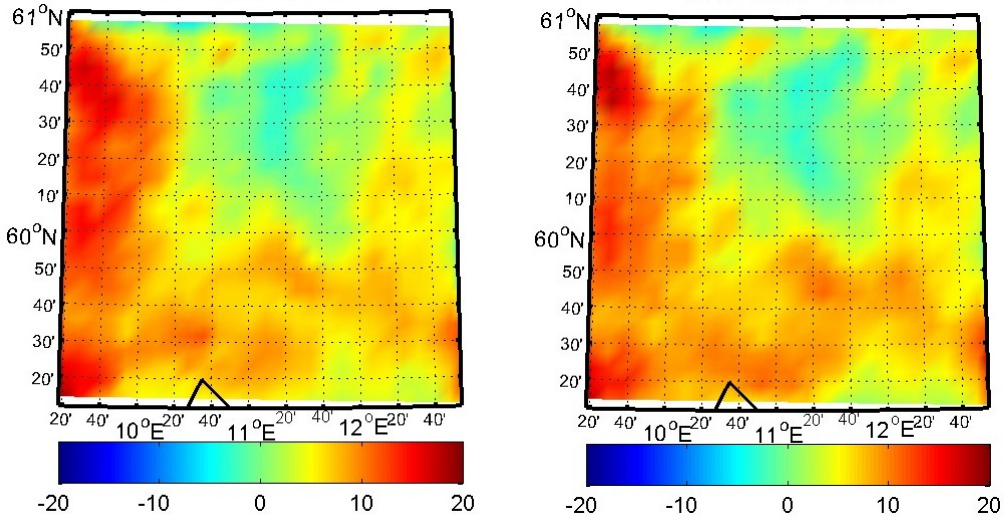

Figure 3.1.8: Change of 10-year return levels (*mm/day*): values related to the period 2021-2050 minus values related to 1971-2000, for winter (left) and summer (right).

3.2 Test case 2: Pizzo d'Alvano (Italy)

This paragraph contains a description of the results related to the test case 2 (Pizzo d'Alvano, Italy). The location is shown in Fig. 3.2.1

Climate of the period 1971-2000 and climate projections over 2021-2050

Fig. 3.2.2 shows the climatology of two-metre temperature over the period 1971-2000 for winter (left) and summer (right). Similarly, Fig. 3.2.3 shows the distribution of total precipitation for winter (left) and summer (right). Fig. 3.2.4 shows the variation of two-metre temperature obtained by subtracting the values on the period 2021-2050 from the values on the period 1971-2000 for winter (left) and summer (right). It is evident that an increase of temperature of about 1^{o} *C* is projected in winter over the whole region, and of about 1.5^{o} *C* in the north-east part of the domain.
Similarly, Fig. 3.2.5 shows the variation of total precipitation (future vs. past) for winter (left) and summer (right). In winter, strong increases of precipitation are expected in the area of Pizzo d'Alvano, while in summer slight reductions are expected over the whole domain.
Figure 3.2.6 shows the histogram of precipitation (past and future period) in the central part of the domain, for winter (left) and summer (right). As we can see in the histogram, no events above 50 *mm* are simulated by the model in that region. To analyse future changes in extreme events with a return period of 10 years, an extreme value analysis is then applied.

Extreme events analysis

Figure 3.2.7 shows the spatial pattern of the 10-year return levels for the period 1971-2000 for winter (left) and summer (right). In winter we see the largest intensities of extreme events in the area of Pizzo d'Alvano (south-central part of the domain), but very strong events are simulated also in large parts of the domain. Figure 3.2.8 shows the changes of the 10-year return levels for the period 2021-2050 with respect to 1971-2000, for winter (left) and summer (right): in the future period (winter), increases of the intensity of extreme events are projected in the north west part of the domain and along the western coastline, whereas decreasing trends are found elsewhere. A quite similar behaviour is simulated in summer.

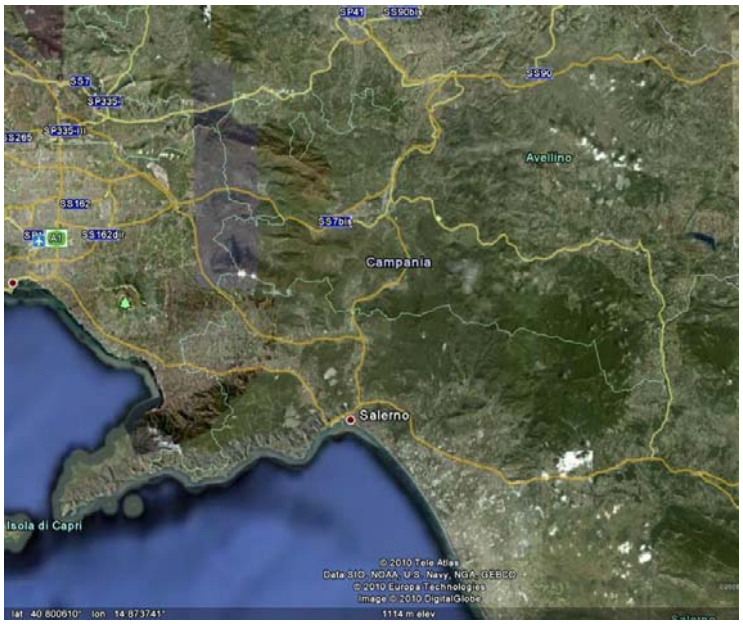

Figure 3.2.1: Location of the site related to test case 2.

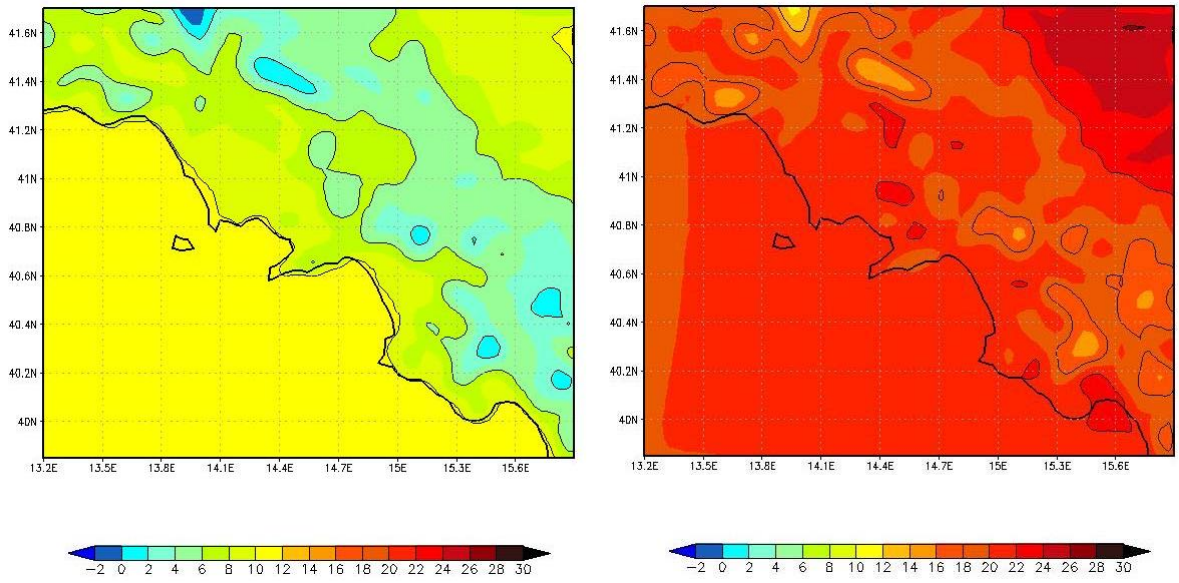

Figure 3.2.2: Two-metre temperature (^oC), averaged on the time period 1971-2000, for winter (left) and summer (right).

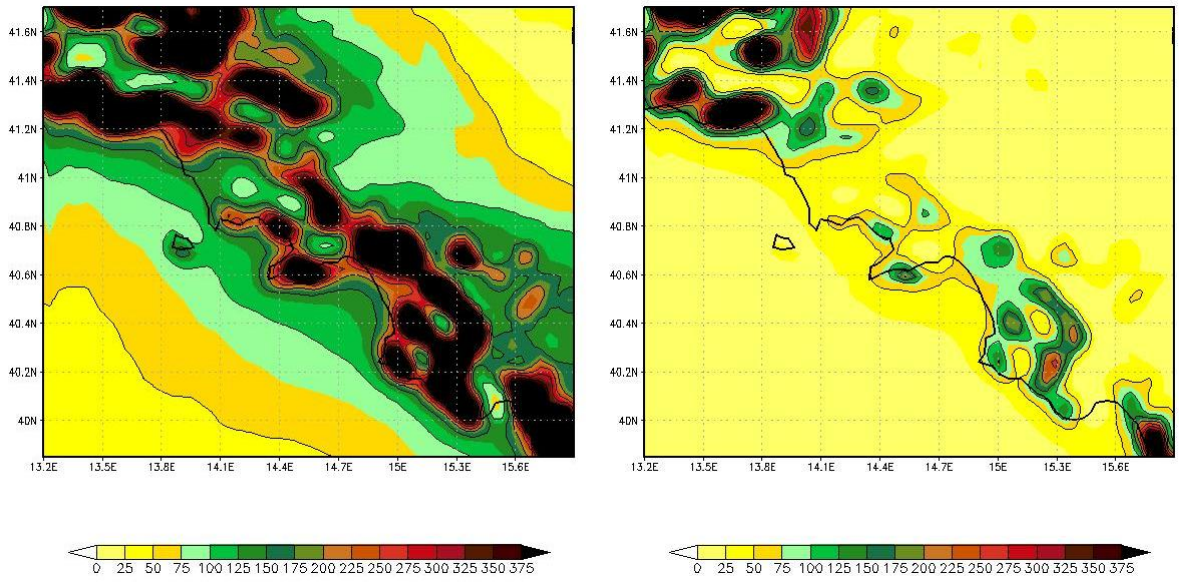

Figure 3.2.3: Total precipitation (*mm/month*), averaged on the time period 1971-2000, winter (left), summer (right).

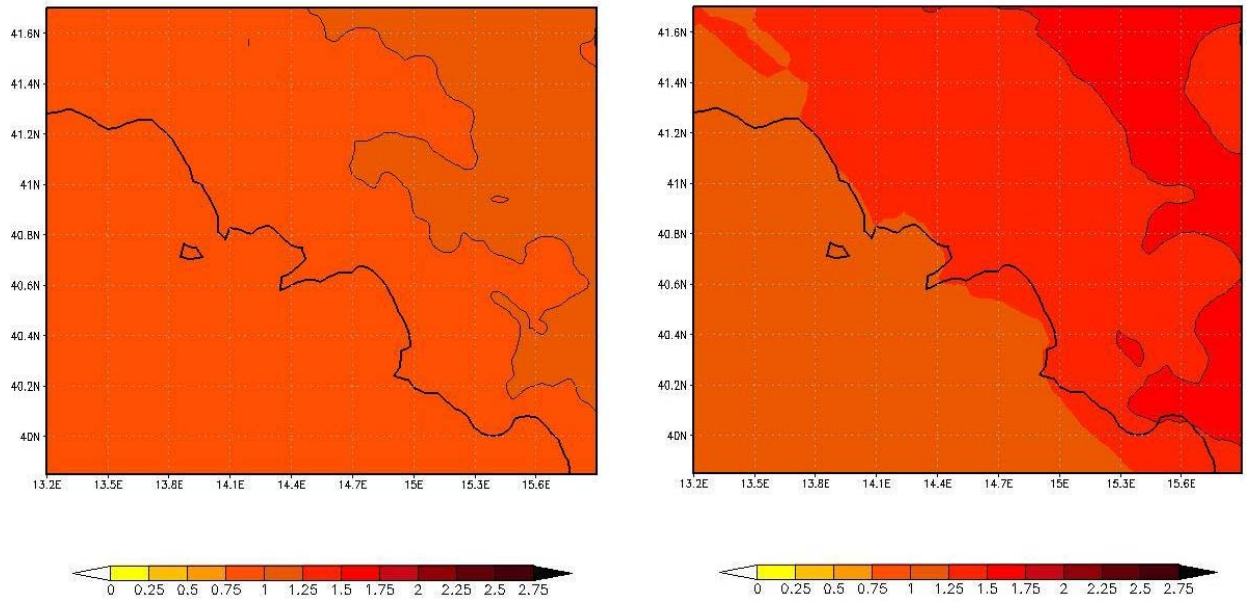

Figure 3.2.4: Change of two-metre temperature (^oC): average values on the period 2021-2050 minus average values on period 1971-2000, for winter (left) and summer (right).

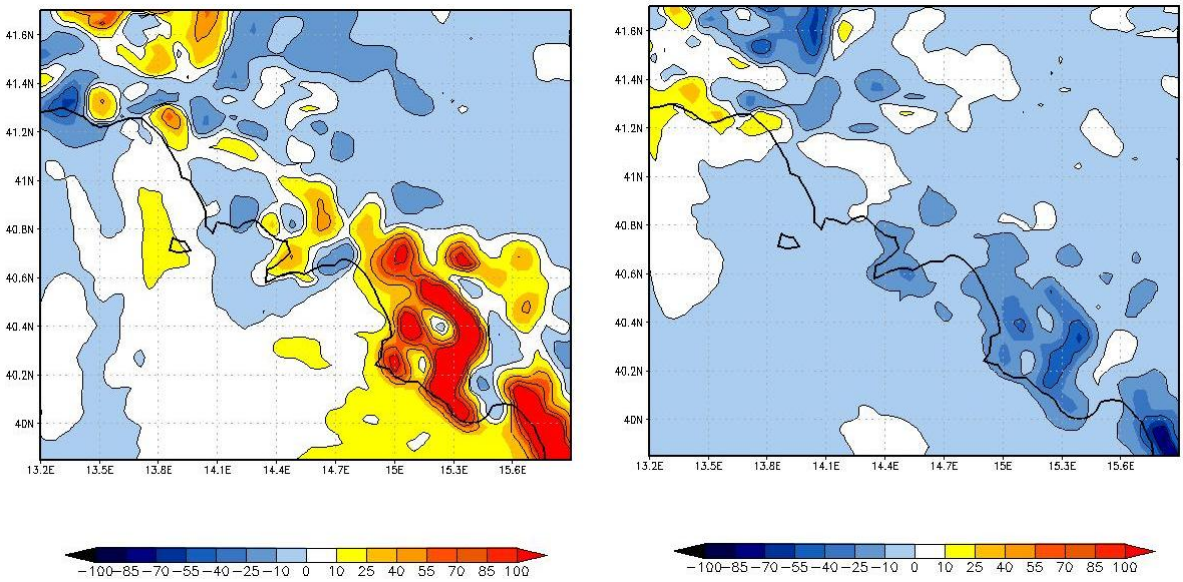

Figure 3.2.5: Change of total precipitation (*mm/month*): average values on the period 2021-2050 minus average values on period 1971-2000, for winter (left) and summer (right).

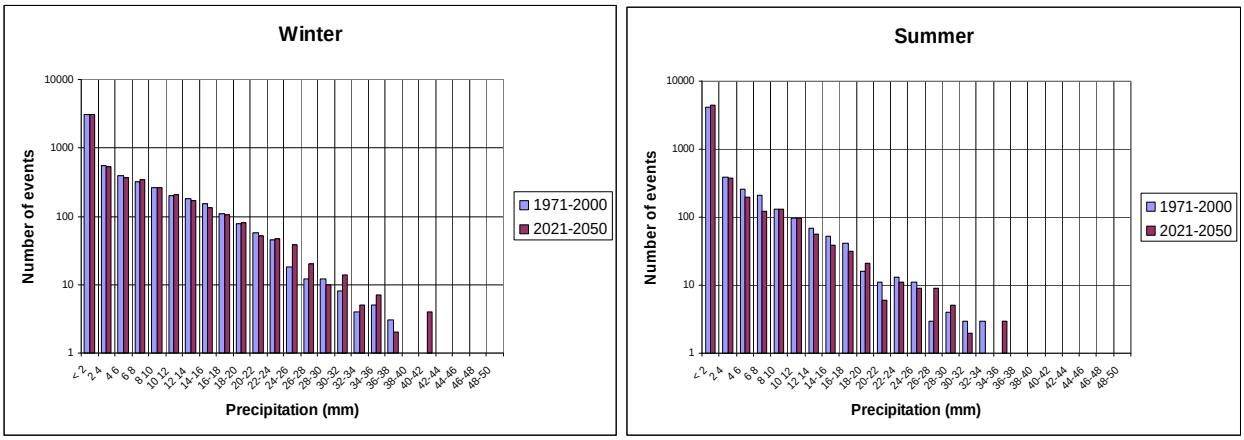

Figure 3.2.6: Histogram of total precipitation related to for winter (*left*), summer (*right*), periods 1971-2000 and 2021-2050.

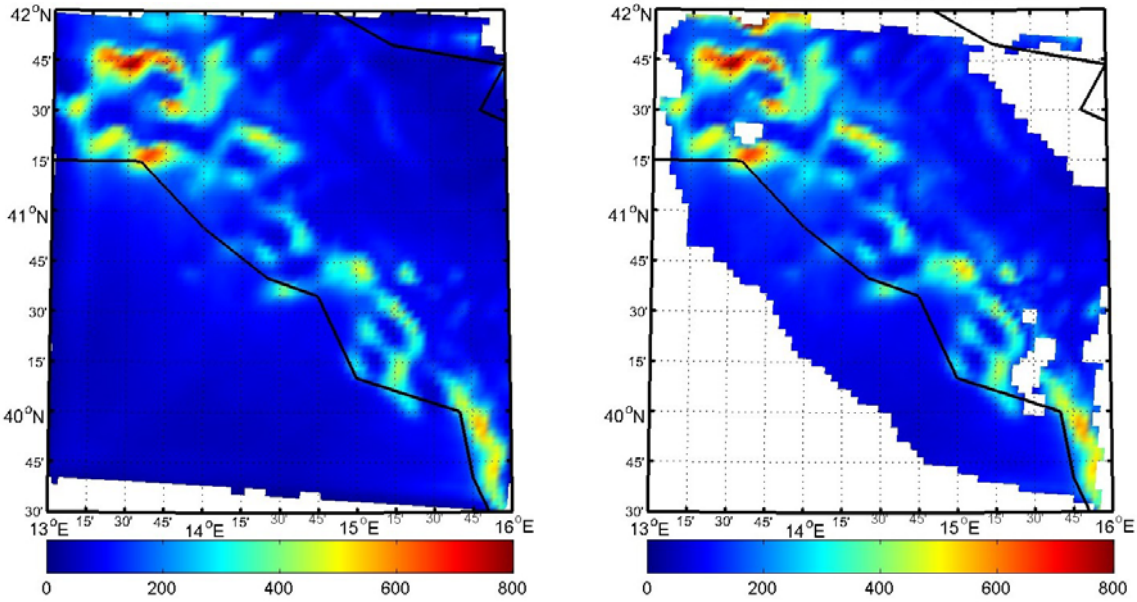

Figure 3.2.7: 10-year return levels (*mm/day*) related to the period 2021-2050 for winter (left) and summer (right).

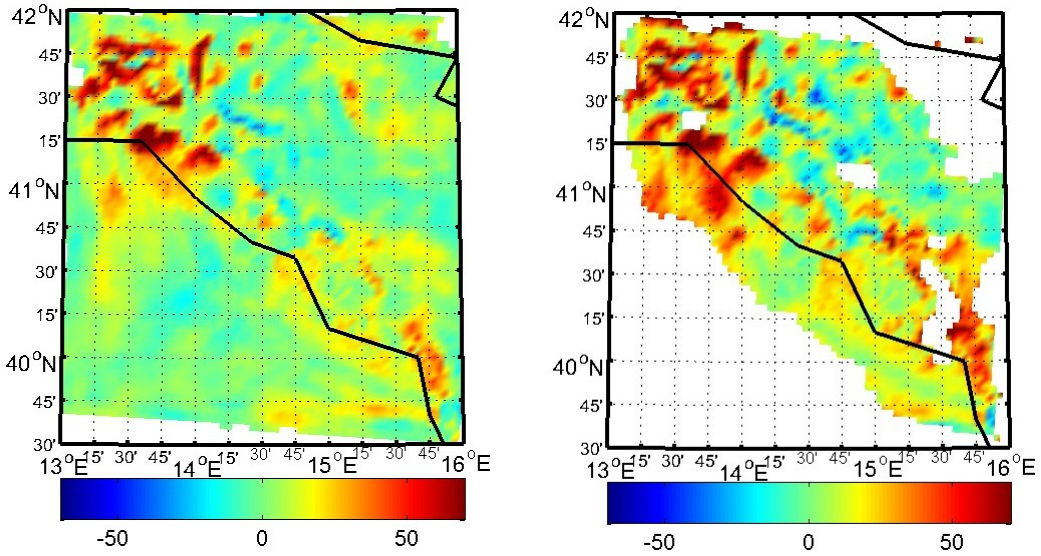

Figure 3.2.8: Change of 10-year return levels (*mm/day*): values related to the period 2021-2050 minus values related to 1971-2000, for winter (left) and summer (right).

3.3 Test case 3: Barcellonette (France)

This paragraph contains a description of the results related to the test case 3 (Barcellonette, France). The location is shown in Fig. 3.3.1 (taken from Google Earth).

Climate of the period 1971-2000 and climate projections over 2021-2050

Fig. 3.3.2 shows the climatology of two-metre temperature over the period 1971-2000 for winter (left) and summer (right). Similarly, Fig. 3.3.3 shows the distribution of total precipitation for winter (left) and summer (right). Fig. 3.3.4 shows the variation of two-metre temperature obtained by subtracting the values on the period 2021-2050 from the values on the period 1971-2000 for winter (left) and summer (right). Significant increases of temperature are registered, up to 3^o *C*, in both seasons, but especially in winter.
Similarly, Fig. 3.3.5 shows the variation of total precipitation (future vs. past) for winter (left) and summer (right). An increase of precipitation of about 25 *mm/month* is expected in winter in the area of Barcellonette, and in small regions in both the seasons; small reductions are registered in wide parts of the domains in summer. Figure 3.3.6 shows the histogram of precipitation (past and future period) in the area of Barcellonette, for winter (left) and summer (right). From these pictures, we see that the number of precipitation events above 50 mm is larger in summer but is projected to slightly increase in both the seasons, especially in winter.

Analysis of extreme events

Figure 3.3.7 shows the spatial pattern of the 10-year return levels for the period 1971-2000 for winter (left) and summer (right). In winter we see the largest intensities of extreme events in the south-west part of the domain, while in summer strong events are observed only on the boundaries. Figure 3.3.8 shows the changes of the 10-year return levels for the period 2021-2050 with respect to 1971-2000, for winter (left) and summer (right): in winter, a slight reduction of heavy precipitation events is projected in the south-west part of the domain and a slight increase in the south-east part of the domain. Since these coincide with a maximum and a minimum in the simulated 10-year return levels during the period 1971-2000 (Figure 3.3.7), this might indicate a shift of heavy precipitation events to the east. In summer, the picture is similar: positive changes are found where heavy precipitation has a minimum and negative where it has a maximum.

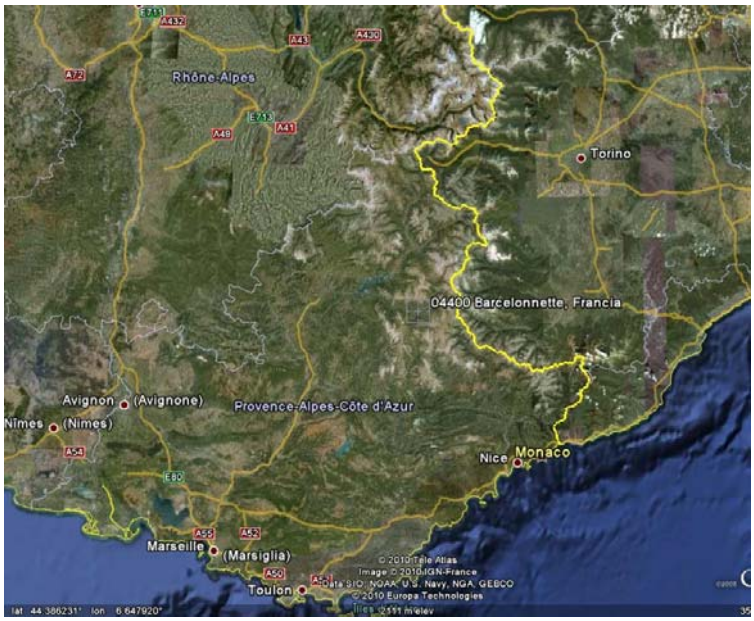

Fig. 3.3.1: Location of the site related to test case 3

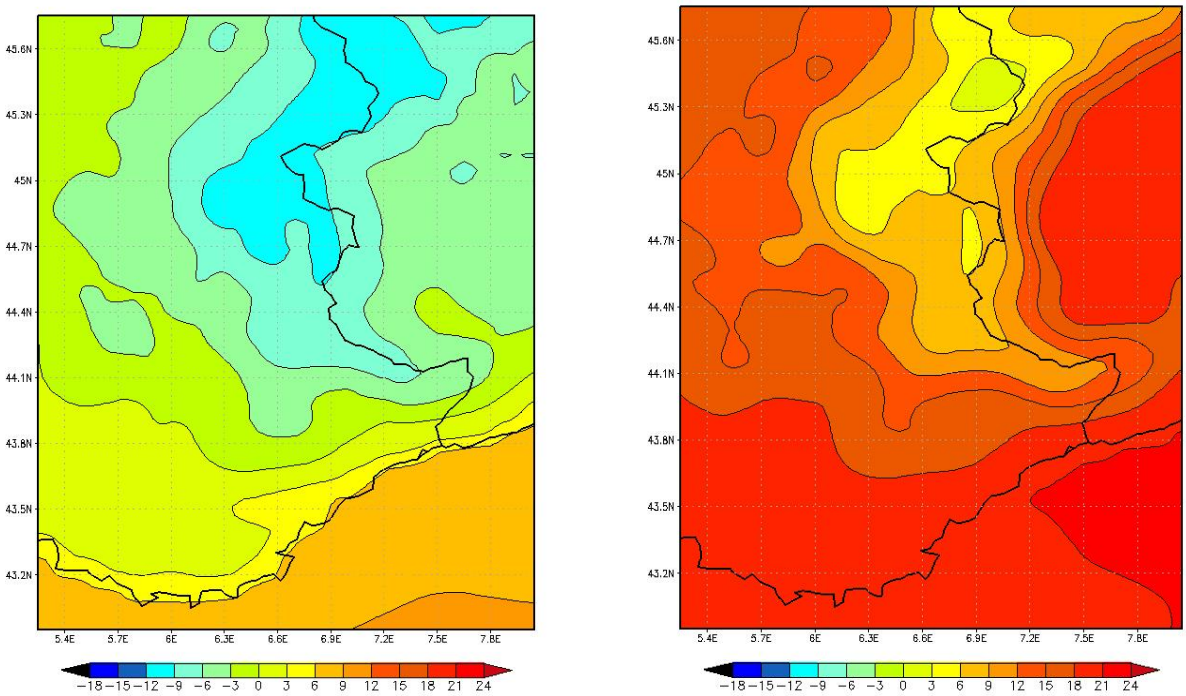

Figure 3.3.2: Two-metre temperature (^oC), averaged on the time period 1971-2000, for winter (left) and summer (right).

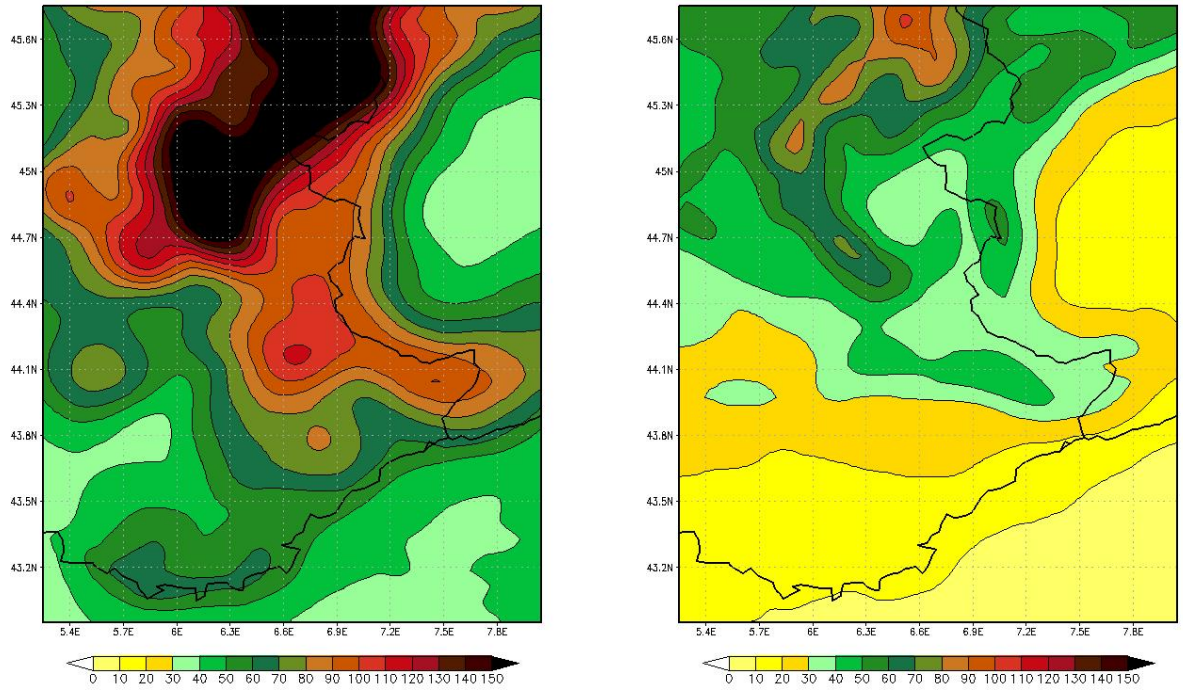

Figure 3.3.3: Total precipitation (*mm/month*), averaged on the time period 1971-2000 for winter (left) and summer (right).

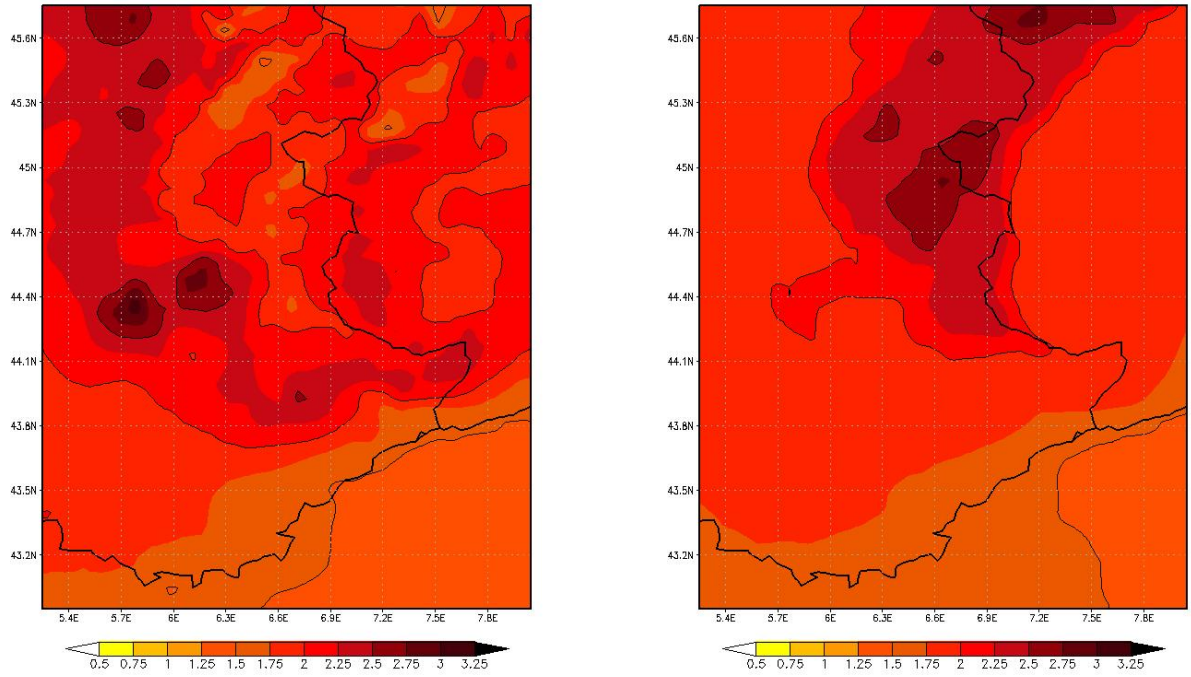

Figure 3.3.4: Change of two-metre temperature (^oC): average values on the period 2021-2050 minus average values on period 1971-2000 for winter (left) and summer (right).

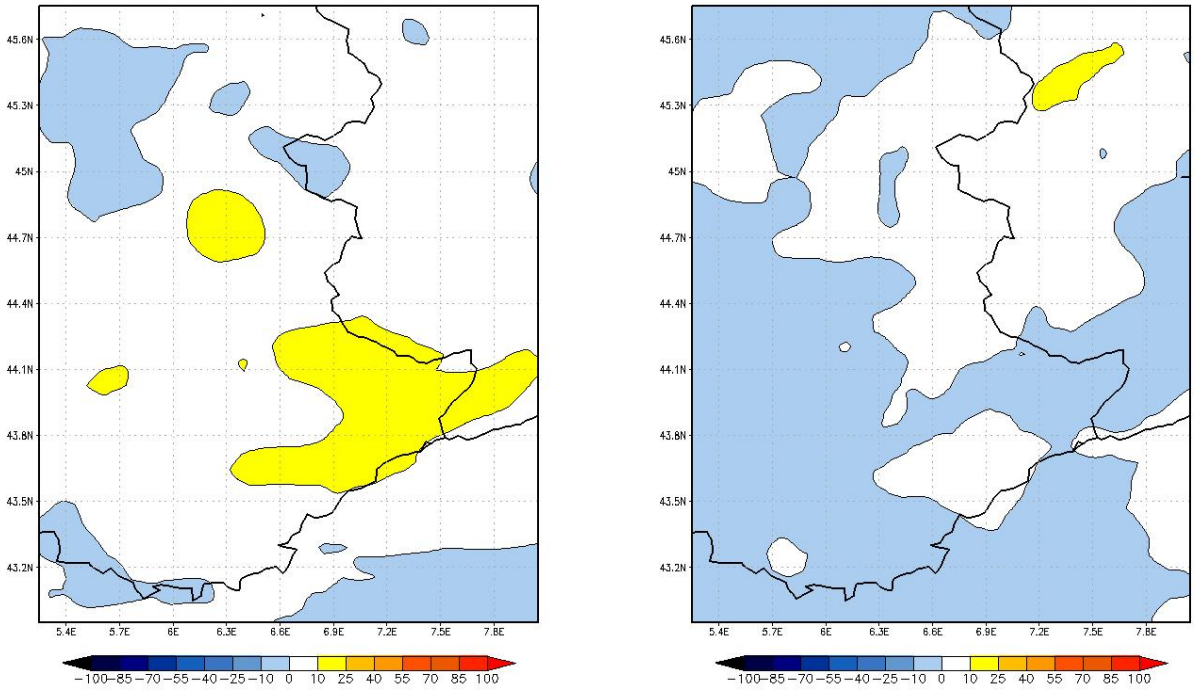

Figure 3.3.5: Change of total precipitation (*mm/month*): average values on the period 2021-2050 minus average values on period 1971-2000, for winter (left) and summer (right).

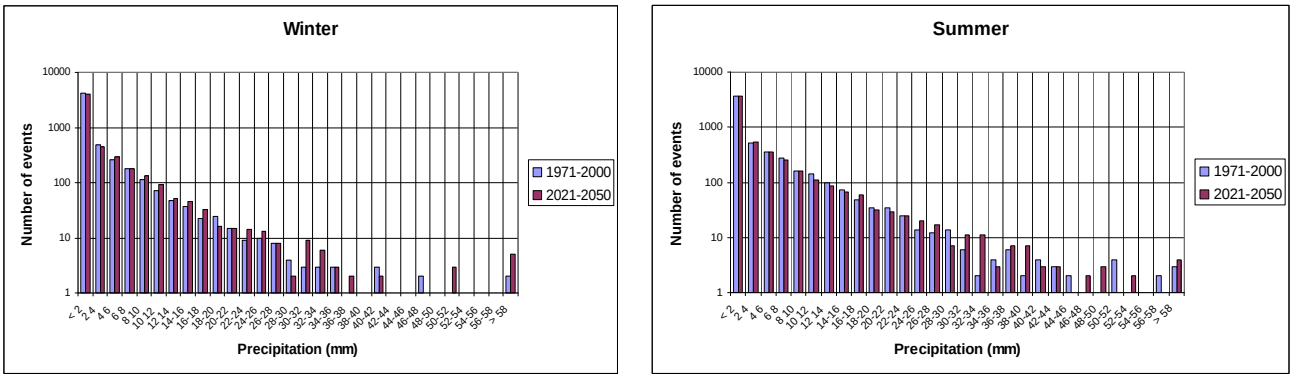

Figure 3.3.6: Histogram of total precipitation related to for winter (*left*), summer (*right*), periods 1971-2000 and 2021-2050.

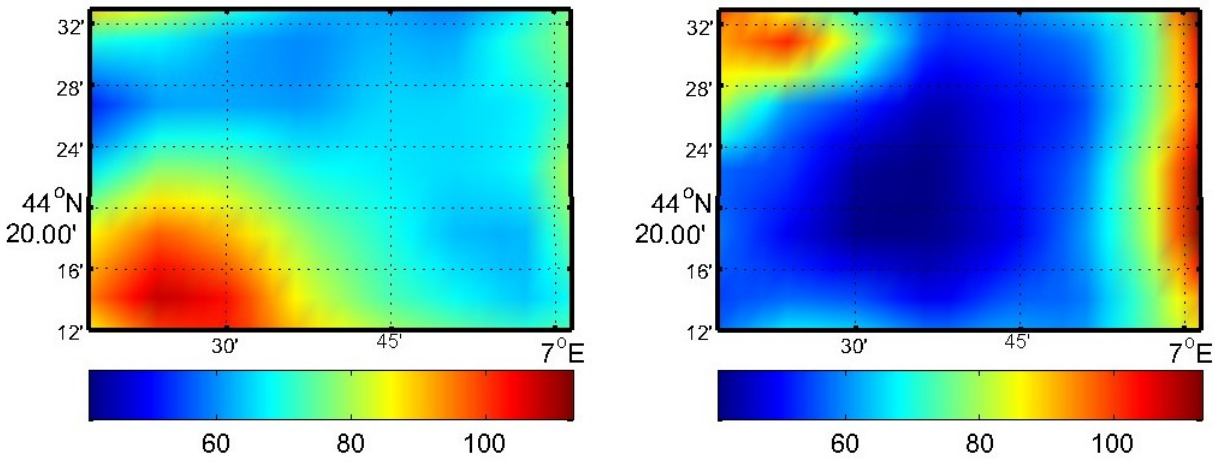

Figure 3.3.7: 10-year return levels (*mm/day*) related to the period 1971-2000 for winter (left) and summer (right)

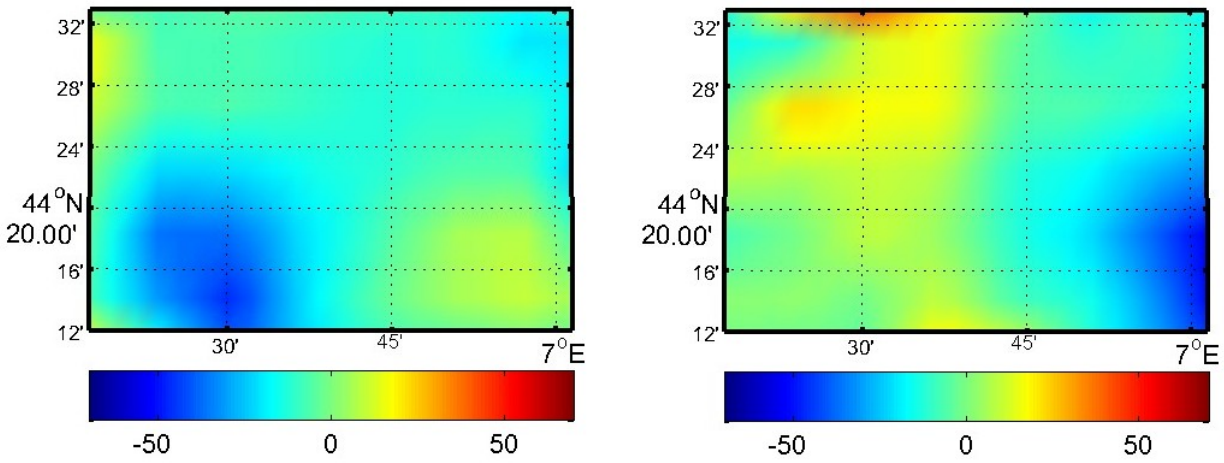

Figure 3.3.8: Change of 10-year return levels (*mm/day*): values related to the period 2021-2050 minus values related to 1971-2000, for winter (left) and summer (right).

3.4 Test case 4: Telega (Romania)

This paragraph contains a description of the results related to the test case 4 (Telega, Romania). The location is shown in Fig. 3.4.1(taken from Google Earth).

Climate of the period 1971-2000 and climate projections over 2021-2050

Fig. 3.4.2 shows the climatology of two-metre temperature averaged over the period 1971-2000 for winter (left) and summer (right). Similarly, Fig. 3.4.3 shows the distribution of total precipitation for winter (left) and summer (right). Fig. 3.4.4 shows the variation of two-metre temperature obtained by subtracting the values on the period 2021-2050 from the values on the period 1971-2000 for winter (left) and summer (right). A general increase of temperature of about 1.5^{o} *C* is expected over the whole domain, for both the seasons.
Similarly, Fig. 3.4.5 shows the variation of total precipitation for winter (left) and summer (right). In winter, in the area of Telega an increase of precipitation is expected, generally about 25 *mm*, with peaks of 70 *mm*, while a general significant reduction is expected in summer.
Figure 3.4.6 shows the histogram of precipitation (past and future period) in the central part of the domain for winter (left) and summer (right): no events above 50 *mm* are simulated by the model in that region.

Analysis of extreme events
Figure 3.4.7 shows the spatial pattern of the 10-year return levels for the period 1971-2000 for winter (left) and summer (right). This picture shows that extreme precipitation events have been simulated in some areas in the central part of the domain both in winter and in summer. Similarly, Figure 3.4.8 shows the changes of the 10-year return levels for the period 2021-2050 with respect to 1971-2000, for winter (left) and summer (right): a similar pattern of changes is expected for both seasons. Increasing trends occur mainly in the north-west of the domain with the magnitude of changes being higher in winter than in summer. In the south-east part of the domain, where the occurrence of heavy precipitation events is rare (see Figure 3.4.7), no significant trends are found in either of the seasons.

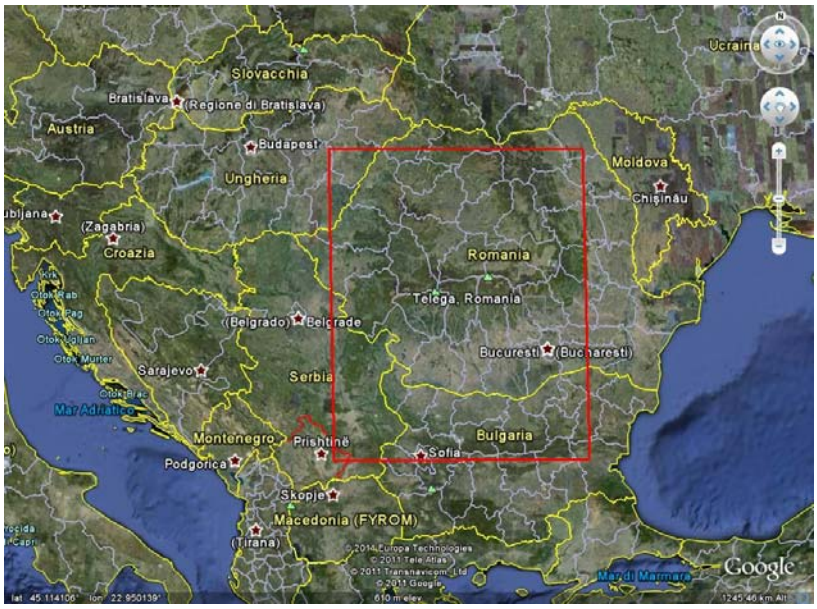

Figure 3.4.1: Location of the site related to test case 4.

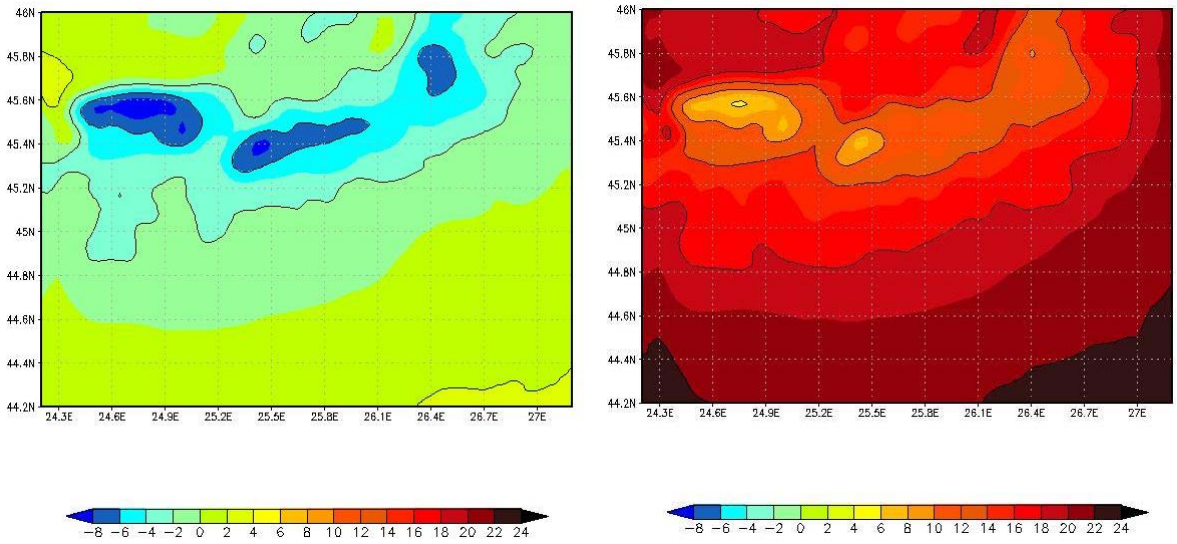

Figure 3.4.2: Two-metre temperature (^oC), averaged on the time period 1971-2000, for winter (left) and summer (right).

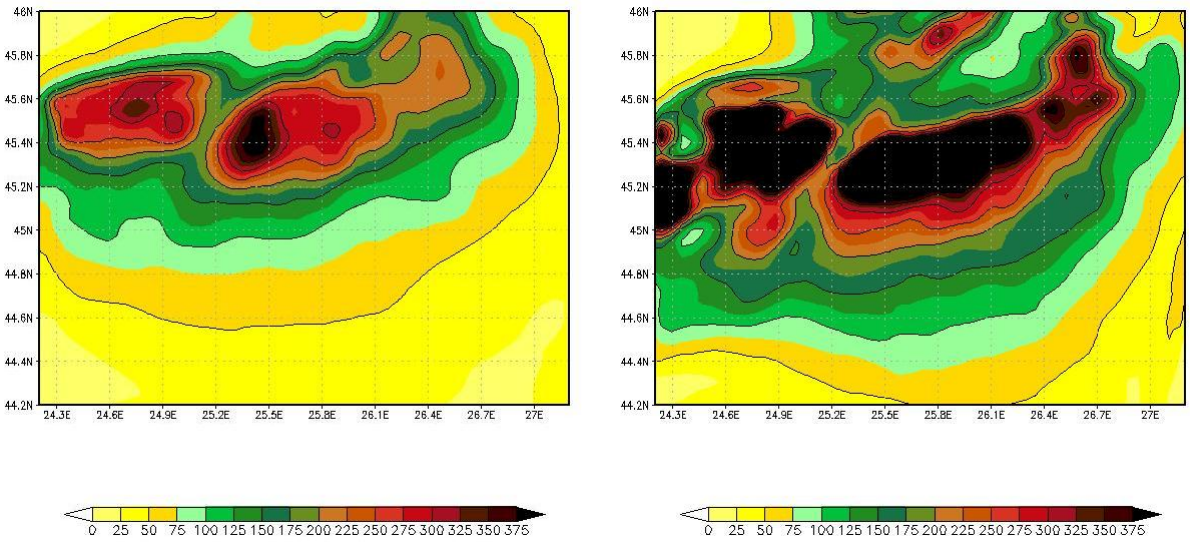

Figure 3.4.3: Total precipitation (*mm/month*), averaged on the time period 1971-2000, for winter (left) and summer (right).

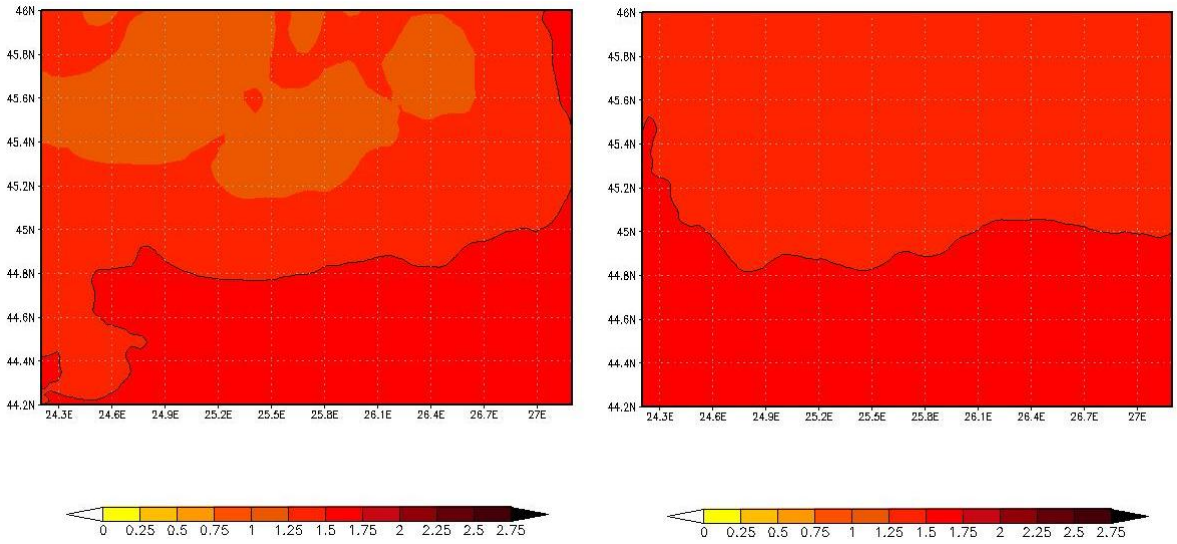

Figure 3.4.4: Change of two-metre temperature (^oC): average values on the period 2021-2050 minus average values on period 1971-2000, for winter (left) and summer (right).

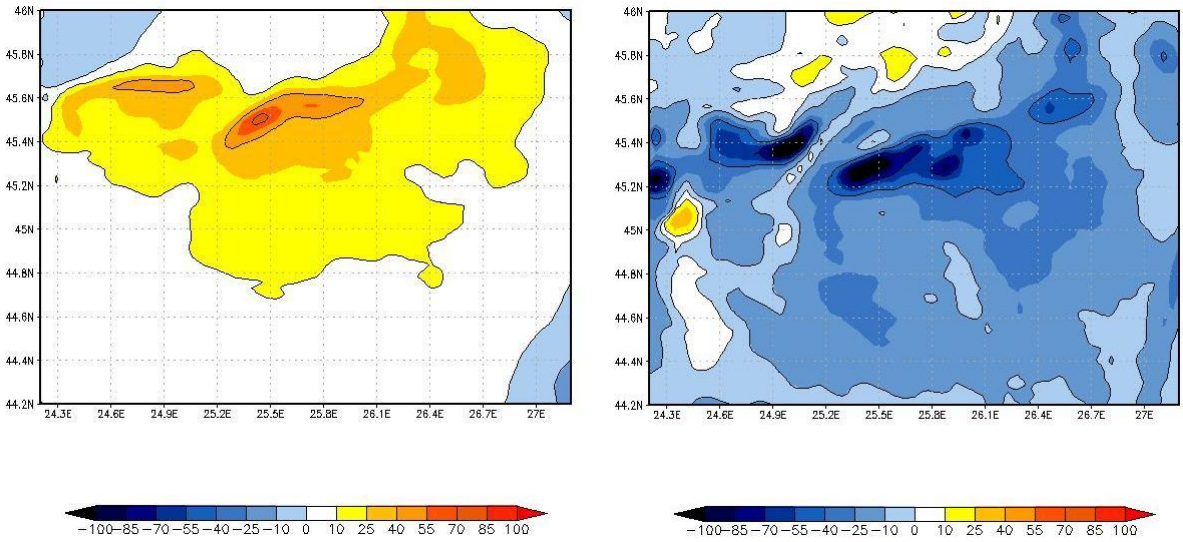

Figure 3.4.5: Change of total precipitation (*mm/month*): average values on the period 2021-2050 minus average values on period 1971-2000, for winter (left) and summer (right).

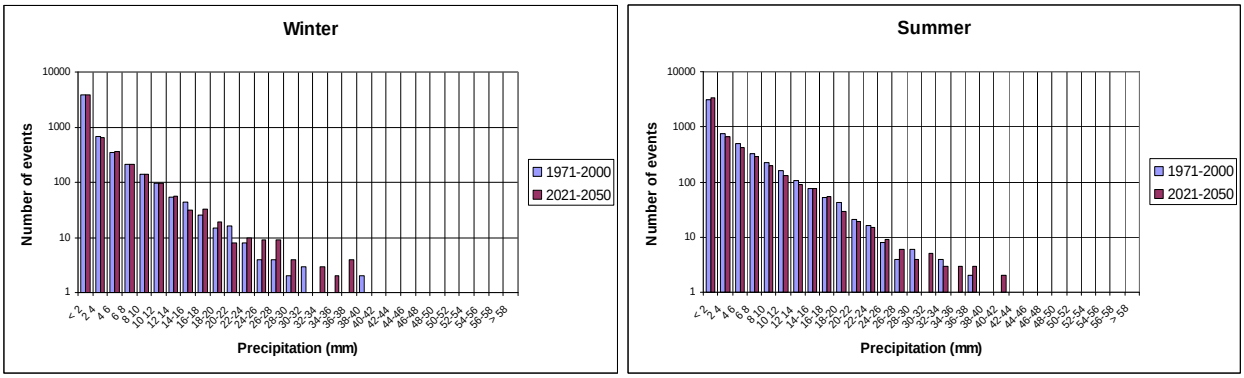

Figure 3.4.6: Histogram of total precipitation related to for winter (*left*), summer (*right*), periods 1971-2000 and 2021-2050.

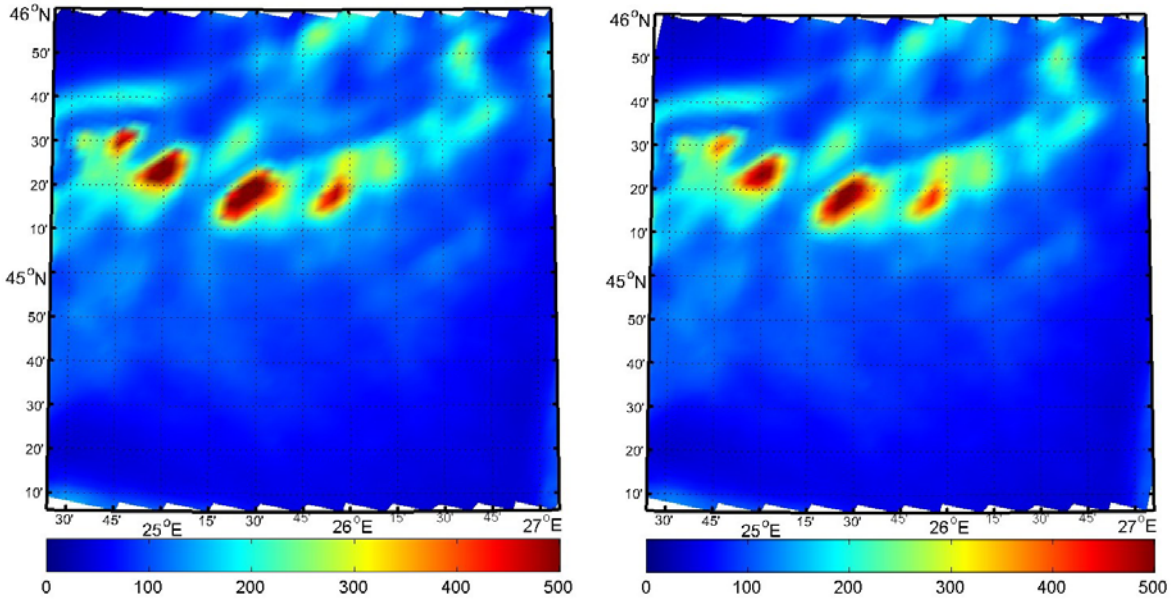

Figure 3.4.7: 10-year return levels (*mm/day*) related to the period 1971-2000 winter (left) and summer (right)

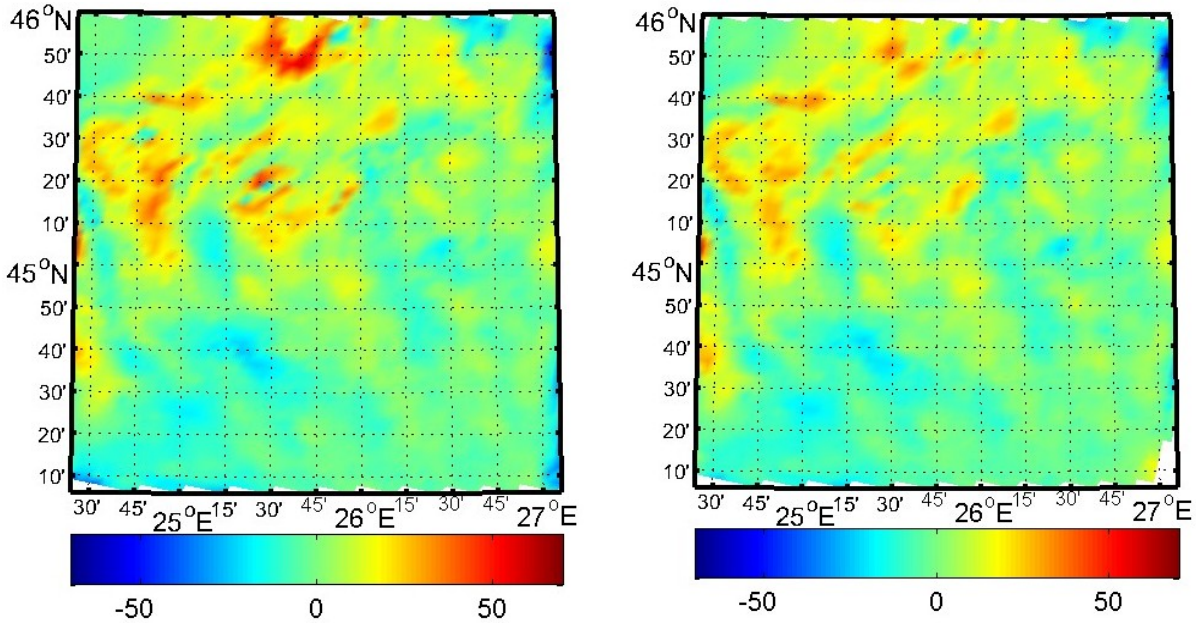

Figure 3.4.8: Change of 10-year return levels (*mm/day*): values related to the period 2021-2050 minus values related to 1971-2000, for winter (left) and summer (right).

4. Conclusions

In the framework of the WP 3.1 of SAFELAND project, high resolution climate simulations have been performed on four areas selected inside Europe, using the regional model COSMO-CLM. The boundary conditions have been obtained in a numerical manner by means of a dynamical *downscaling* technique, using results from the regional climate model REMO provided by MPI-M at a spatial resolution 10 *km*. Simulations have been performed over the time period 1951-2050, employing the SRES A1B emission scenario. Results of two-metre temperature and total precipitation averaged over the time periods 1971-2000 and 2021-2050 have been presented, in order to highlight the variations expected in the future, with respect to the past period.

In the area of Nedre Romerike (Norway) strong increases of temperature are projected especially in winter, while a general increase of precipitation is expected in winter, with a general increase of extreme events which is most pronounced in the western part of the domain.

In the area of Pizzo d'Alvano (Italy), a growth of temperature is also projected, even if less evident than the previous case. In winter, strong increases of precipitation (with strong extreme events) are expected in the area of Pizzo d'Alvano, In summer slight reductions are expected for the average monthly precipitation over the whole domain, which is in contrast to a projected increase in daily precipitation extremes in the Pizzo d'Alvano region and along the western coast line.

In the area of Barcellonette (France) significant increases of temperature are expected in the future, up to $3^o C$, in both seasons, but especially in winter. An increase of precipitations is expected in small sub domains in both seasons, with slight changes of extreme events on the whole domain.

Finally, in the area of Telega (Romania), a general increase of temperature of about $1.5^o C$ is expected over the whole domain, for both the seasons. In winter an increase of precipitation is expected, while a general significant reduction is expected in summer; an increase of extreme events is expected in winter and summer in the north of the domain with the magnitude of the changes being higher in winter.

REFERENCES

[1] Coles, S., 2001. An Introduction to Statistical Modeling of Extreme Values. Springer, 208 pages.
[2] Holton, J.R. 2004. *An introduction to Dynamic Meteorology*, Elsevier Academic Press.
[3] Kain J.S., J.M. Fritsch, 1993. Convective parameterization for mesoscale models: the Kain-Fritsch scheme, *Meteorol. Monographs* 24: 165-170.
[4] Naveau, P., M. Nogaj, C. Ammann, P. Yiou, D. Cooley, and V. Jomelli, 2005, Statistical methods for the analysis of climate extremes. *Comptes rendus Geosciences de l'Academie des Sciences*, 1013–1022.
[5] Rockel, B., A. Will, A. Hense, 2008. The regional Climate Model COSMO-CLM (CCLM), *Meteorologische Zeitschrift*, 17 (4): 347-348.
[6] Solomon, S., D. Qin, M. Manning, Z. Chen, M. Marquis, K.B. Averyt, M. Tignor, and H.L. Miller. *Climate Change 2007: The Physical Science Basis. Contribution of Working Group I to the Fourth*

Assessment Report of the Intergovernmental Panel on Climate Change. Cambridge University Press, Cambridge, United Kingdom and New York, NY, USA..
[7] Tiedtke, M. 1989. A comprehensive mass flux scheme for cumulus parameterization in large scale models, *Mon. Wea. Rev*., 117: 1779-1800.